

Deep Archetypal Analysis

Sebastian Mathias Keller¹ Maxim Samarin¹ Mario Wieser¹ Volker Roth¹

Abstract

“Deep Archetypal Analysis” generates latent representations of high-dimensional datasets in terms of fractions of intuitively understandable basic entities called archetypes. The proposed method is an extension of linear “Archetypal Analysis” (AA), an unsupervised method to represent multivariate data points as sparse convex combinations of extremal elements of the dataset. Unlike the original formulation of AA, “Deep AA” can also handle side information and provides the ability for data-driven representation learning which reduces the dependence on expert knowledge. Our method is motivated by studies of evolutionary trade-offs in biology where archetypes are species highly adapted to a single task. Along these lines, we demonstrate that “Deep AA” also lends itself to the supervised exploration of chemical space, marking a distinct starting point for de novo molecular design. In the unsupervised setting we show how “Deep AA” is used on CelebA to identify archetypal faces. These can then be superimposed in order to generate new faces which inherit dominant traits of the archetypes they are based on.

1. Introduction

The evolutionary development of biological systems is characterized by a fundamental trade-off: If multiple tasks need to be performed, no system can be optimal at all tasks at once. Examples of such trade-offs include those between longevity and fecundity in *Drosophila melanogaster* where long-lived flies show decreased fecundity (Djawdan et al., 1996) or predators that evolve to be fast runners but eventually have to trade-off their ability to subdue large or strong prey, e.g. cheetah versus lion (Garland, 2014). Such evolutionary trade-offs are known to affect the range of phenotypes found in nature (Tendler et al., 2015). In (Shoval et al., 2012) empirical examples are presented to support the

¹Department of Mathematics and Computer Science, University of Basel, Switzerland. Correspondence to: Sebastian Keller <sebastianmathias.keller@unibas.ch>.

argument that best–trade-off phenotypes are weighted averages of archetypes where archetypes are understood to be phenotypes specialized for a single task. An example of an evolutionary trade-off in the space of traits (or phenospace) for 138 species of bats (Microchiroptera) is shown in Fig. 1. Based on data from (Norberg et al., 1987) the dominant food habit of each species is represented in a two-dimensional space where the axis depict *Body Mass* and *Wing Aspect Ratio*. The latter is the square of the wingspan divided by the wing area. The indicated archetypes were calculated according to Archetypal Analysis proposed by (Cutler & Breiman, 1994). Table 1 gives an account of the *single* task a given archetype is optimized to perform. The trade-off situation

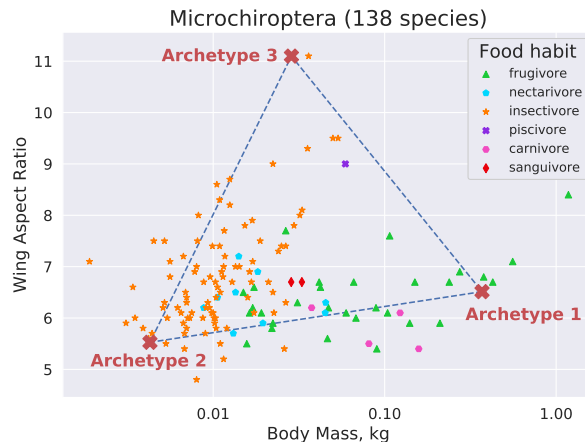


Figure 1. Phenospace of 138 species of Microchiroptera. The dominant food habit of each species, and thereby the ability to procure this food source, is linked to the morphology of the animals, e.g. a higher *Wing Aspect Ratio* corresponds with the greater aerodynamic efficiency needed to chase high flying insects. Archetypes are extreme types, optimized to perform a single task. Proximity of a species to an archetype quantifies the level of adaptation this species has undergone with respect to the archetypal task.

can be interpreted using Pareto optimality theory (Steuer, 1986) which was recently used in biology to study trade-offs in evolution (Schuetz et al., 2012; El Samad et al., 2005). All phenotypes that have evolved over time lie within a restricted part of the phenospace, the so-called Pareto front, which is the set of phenotypes that cannot be improved at all tasks simultaneously. If there were a phenotype p being better at all tasks than a second phenotype p' then the latter would be eliminated by natural selection. Consequently phenotypes

Table 1. Characteristic traits of the archetypes identified in Fig. 1 and the task each archetypal species is optimized to perform.

ARCHETYPE	TRAITS	TASK: HUNT FOR...
ARCHETYPE 1	LOW ASPECT RATIO, LARGE BODY	...PLANT MATERIAL, NECTAR & POLLEN
ARCHETYPE 2	LOW ASPECT RATIO, SMALL BODY	...SMALL INSECTS NEAR VEGETATION
ARCHETYPE 3	HIGH ASPECT RATIO, MEDIUM BODY	...HIGH FLYING, LARGE INSECTS

on the Pareto front are the best possible compromises between the different requirements or tasks. However, there are several shortcomings associated with Archetypal Analysis: (i) Regarding the Microchiroptera example, a total of eight measurements per species were collected by (Norberg et al., 1987) but selecting the dimensions that would reveal the relation between food habit and phenotype depicted in Fig. 1 requires prior knowledge, here in form of knowledge about aerodynamics. (ii) A representational problem is introduced when features of different types and from different domains are used. Again referring to Fig. 1, representing the *Body Mass* on a log-scale while the *Wing Aspect Ratio* enters linearly requires expert knowledge or is simply the result of a trial and error process if even a domain expert cannot provide useful insights. (iii) Finally, Archetypal Analysis in its original formulation is an *unsupervised* learning process, i.e. side information cannot be taken into account during learning.

Literature “Archetypal Analysis” (AA) was first proposed by Adele Cutler and Leo Breiman (Cutler & Breiman, 1994). Since its conception AA has known several advancements on the algorithmic as well as the application side. An extension to Kernel AA is proposed by (Bauckhage & Manshaei, 2014), algorithmic improvements by adapting a Frank–Wolfe type algorithm to calculate the archetypes are made by (Bauckhage et al., 2015) and the extension by (Seth & Eugster, 2016) introduces a probabilistic version of AA. In (Prabhakaran et al., 2012) the authors are concerned with model selection by asking for the optimal number of archetypes for a given dataset while (Kaufmann et al., 2015) addresses in part the shortcoming of AA we describe in the introduction under (ii). Although AA did not prevail as a commodity tool for pattern analysis it has for example been used by (Bauckhage & Thureau, 2009) to find archetypal images in large image collections or by (Canhasi & Kononenko, 2015) to perform the analogous task for large document collections. For the human genotype data studied by (Huggins et al., 2007), inferred archetypes are interpreted as representative populations for the measured genotypes. And in (H. P. Chan et al., 2003) AA is used to analyse galaxy spectra which are viewed as weighted superpositions of the emissions from

stellar populations, nebular emissions and nuclear activity. Variational Autoencoders (VAEs), arguably the post prevalent representatives of the class of “Deep Latent Variable Models”, were introduced by Kingma & Welling (2013); Rezende et al. (2014) and use an inference network to estimate a variational lower bound of the posterior distribution of the latent variable. Important work in this direction include Kingma et al. (2014); Rezende & Mohamed (2015) and Jang et al. (2017). More recently, (Alemi et al., 2016) has discovered a close connection between VAE and the Information Bottleneck principle (Tishby et al., 2000a). Here, the Deep Information Bottleneck (DIB) is a VAE where X is replaced by Y in the decoder. Subsequently, the DIB has been extended in multiple directions such as sparsity (Wieczorek et al., 2018) or causality (Parbhoo et al., 2018).

Contribution We propose *Deep Archetypal Analysis* (DeepAA) which is a novel, non-linear extension of the original model proposed by (Cutler & Breiman, 1994). By introducing *DeepAA* within a VAE framework we address several issues of the original model. Unlike the original model, *DeepAA* (i) does not rely on expert knowledge when combining relevant dimensions, (ii) learns appropriate transformations (e.g. scaling) when combining features of different types and (iii) is able to incorporate side information into the learning process if necessary. Beside the analysis of evolutionary trade-offs as the motivation for *DeepAA*, we present two large scale experiments: First we show that the unsupervised exploration of CelebA (Liu et al., 2015) using *DeepAA* offers a highly interpretable perspective on the dominant factors of variation as face images can be characterized as convex mixtures of *archetypal faces*. Second we demonstrate the usefulness of *DeepAA* in a setting with side information on the QM9 dataset which contains the chemical structures and properties of 134 kilo molecules (Ruddigkeit et al., 2012; Ramakrishnan et al., 2014). As modern chemistry and material science are increasingly concerned with material property prediction, we show that *DeepAA* can be used to *systematically* explore vast chemical spaces in order to identify starting points for further chemical optimisation.

2. Archetype-VAE Framework

In the following we will use *linear* AA when referring to the original archetype model from (Cutler & Breiman, 1994).

2.1. Linear Archetypal Analysis

Linear AA is a form of non-negative matrix factorization where a matrix $X \in \mathbb{R}^{n \times p}$ of n data vectors is approximated as $X \approx ABX = AZ$ where $A \in \mathbb{R}^{n \times k}$ and $B \in \mathbb{R}^{k \times n}$, usually with $k < \min\{n, p\}$. The matrices A and B are row-stochastic weight matrices, while the matrix $Z \in \mathbb{R}^{k \times p}$, known as the archetype matrix, contains k

archetypes $\mathbf{z}_1, \dots, \mathbf{z}_j, \dots, \mathbf{z}_k$. The model is subject to the following constraints:

$$a_{ij} \geq 0 \wedge \sum_{j=1}^k a_{ij} = 1, \quad b_{ji} \geq 0 \wedge \sum_{i=1}^n b_{ji} = 1 \quad (1)$$

Constraining the entries of A and B to be non-negative and demanding that both matrices be row stochastic, implies a representation of the data vectors $\mathbf{x}_{i=1..n}$ as a weighted sum of the rows of Z (=archetypes) while simultaneously representing the archetypes $\mathbf{z}_{j=1..k}$ themselves as a weighted sum of the n data vectors in X :

$$\mathbf{x}_i \approx \sum_{j=1}^k a_{ij} \mathbf{z}_j = \mathbf{a}_i Z, \quad \mathbf{z}_j = \sum_{i=1}^n b_{ji} \mathbf{x}_i = \mathbf{b}_j X \quad (2)$$

Due to the constraints on A and B in Eq. 1 both the representation of \mathbf{x}_i and \mathbf{z}_j in Eq. 2 are *convex* combinations. Therefore the archetypes approximate the data convex hull and increasing the number k of archetypes improves this approximation. The central problem of AA is finding the weight matrices A and B for a given data matrix X .

AA is most appropriate and provides meaningful interpretations especially in cases where a dataset is believed to be a superposition of *basic* or *pure* entities. ϵ used to provide a lower dimensional representation of the data.

2.2. Deep Archetypal Analysis

In the following we intentionally use a different notation as *DeepAA* is a probabilistic model unlike linear AA.

The Deep Variational Information Bottleneck introduced by (Alemi et al., 2016) combines the information bottleneck (IB) from (Tishby et al., 2000b) with the VAE approach (Kingma & Welling, 2013). The objective of the IB method is to find a random variable T which, while compressing a given random vector X , preserves as much information about a second given random vector Y . The objective function of the IB is as follows

$$\min_{p(t|x)} I(X; T) - \lambda I(T; Y), \quad (3)$$

where λ is a Lagrange multiplier and I denotes the mutual information. Assuming the IB Markov chain $T - X - Y$ and a parametric form of Eq. 3 with parametric conditionals $p_\phi(t|x)$ and $p_\theta(y|t)$, Eq. 3 is written as

$$\max_{\phi, \theta} -I_\phi(T; X) + \lambda I_{\phi, \theta}(T; Y). \quad (4)$$

Following (Wieczorek et al., 2018), the two terms in Eq. 4 have the following forms:

$$\begin{aligned} I_\phi(T; X) &= D_{KL}(p_\phi(t|x)p(x) \| p(t)p(x)) \\ &= \mathbb{E}_{p(x)} D_{KL}(p_\phi(t|x) \| p(t)) \end{aligned} \quad (5)$$

and

$$\begin{aligned} I_{\phi, \theta}(T; Y) &= D_{KL}\left(\left[\int p(t|y, x)p(y, x) dx\right] \| p(t)p(y)\right) \\ &= \mathbb{E}_{p(x, y)} \mathbb{E}_{p_\phi(t|x)} \log p_\theta(y|t) + h(Y) \end{aligned} \quad (6)$$

Here $h(y) = -\mathbb{E}_{p(y)} \log p(y)$ denotes the entropy of y in the discrete case or the differential entropy in the continuous case. Viewing the model formulated in Eq. 5 as the encoder and the model in Eq. 6 as the decoder, the optimization problem is cast as a VAE. Assuming a simple prior of the form $p(t) = \mathcal{N}(t; 0, I)$, the KL divergence in Eq. 5 becomes a KL divergence between two Gaussian distributions which can be expressed in analytical form. $I_\phi(T; X)$ can then be estimated on (mini-)batches as

$$I_\phi(T; X) \approx \frac{1}{n} \sum_i D_{KL}(p_\phi(t|x_i) \| p(t)). \quad (7)$$

As for the decoder, $\mathbb{E}_{p(x, y)} \mathbb{E}_{p_\phi(t|x)} \log p_\theta(y|t)$ in Eq. 6 is estimated using the reparametrisation trick proposed by (Kingma & Welling, 2013; Rezende et al., 2014):

$$\begin{aligned} I(T; Y) &= \mathbb{E}_{p(x, y)} \mathbb{E}_{\epsilon \sim \mathcal{N}(0, I)} \dots \\ &\dots \sum_j \log p_\theta(y_j | t = \boldsymbol{\mu}_j(x) + \text{diag}(\sigma_j(x))\epsilon) + \text{const.} \end{aligned} \quad (8)$$

Note that without loss of generality we can assume $y = (y', x)$ in Eq. 4. This form will be used in the *Microchiroptera* and the *Chemical Space Exploration* experiment where side information y' is available.

In the following we adopt a probabilistic perspective on AA in order to formulate a constraint which will be used in the IB. The resulting model will be *DeepAA*.

Archetypal Analysis requires the means $\boldsymbol{\mu}_j$ in Eq. 9, i.e. the latent samples in *DeepAA*, to be convex combinations of the archetypes \mathbf{z}_j . But at the same time the archetypes \mathbf{z}_j need to be convex mixtures of the means $\boldsymbol{\mu}_j$. Following (Seth & Eugster, 2016), the generative process for the observations \mathbf{t}_i is as follows:

$$\mathbf{a}_i \sim \text{Dir}_k(\boldsymbol{\alpha}) \quad \wedge \quad \mathbf{t}_i \sim \mathcal{N}\left(\underbrace{\mathbf{a}_i Z}_{\boldsymbol{\mu}_i}, \epsilon^2 \mathbf{I}\right), \quad (9)$$

with $\sum_{j=1}^k \alpha_j = \mathbf{1}' \boldsymbol{\alpha} = 1$. The \mathbf{a}_i are the weights of the archetypes while the observations \mathbf{t}_i are scattered around the means $\boldsymbol{\mu}_i = \mathbf{a}_i Z$ according to isotropic Gaussian noise with variance ϵ^2 .

A major difference to linear AA is that for *DeepAA* we do not need to learn the positions of the archetypes \mathbf{z}_j as there is no absolute frame of reference in latent space. We thus start by positioning $n + 1$ archetypes at the vertex points of a n -simplex and collect these *fixed* coordinates in the matrix

Z^{fixed} . The implication is that learning a weight matrix B to represent the archetypes as a sum over weighted means is – at least in theory – not necessary. Instead we formulate two constraints with respect to the weights \mathbf{a}_i in Eq. 9, resp. the weight matrix A . These are:

- (i) C_1 : A is (row-)stochastic
- (ii) C_2 : most of the mass of $a_{i,\bullet}$ lies in one dimension

The first constraint simply carries over from linear AA while the second ensures that the latent means μ_i do not concentrate at the center of the simplex but also populate regions proximal to the fixed coordinates of the archetypes $\mathbf{z}^{\text{fixed}}$. Formally, we introduce these constraints to the IB in Eq. 4 as follows:

$$\max_{\phi, \theta} -I_{\phi}(T; X) + \lambda I_{\phi, \theta}(T; Y) \quad \text{s.t.} \quad (C_1, C_2) \quad (10)$$

with $I_{\phi}(t; x)$ and $I_{\phi, \theta}(t; y)$ given by the expressions in Eq. 7 and Eq. 8. There are several ways to enforce these constraints. In the next subsection we will shortly present a possible implementation.

2.3. Implementation Details

We force the constraints in Eq. 10 by implementing a new loss function we call *Archetype Loss*, AT-loss for short:

$$\text{loss}_{\text{AT}} = \|\mu^{\text{dir}} - \mu^{\text{pred}}\|_F^2 + \|Z^{\text{fixed}} - Z^{\text{pred}}\|_F^2 \quad (11)$$

The model architecture is shown in Fig. 2. From the last layer of the encoder we learn A_{μ} , B_z , μ^{direct} and the variance. The AT-loss ensures that the predicted archetypes Z^{pred} as convex mixtures of the latent means μ^{dir} are mapped close to the coordinates defined in the matrix Z^{fixed} (analog for μ^{dir}). As a result the weight matrices A and B are estimated. In general, the archetype loss can be small only if input data is mapped closely to the fixed archetypes. One can regard the branch in Fig. 2 containing μ^{direct} and the variance as a vanilla VAE with an *additional* constraint given by the AT-loss and the branch containing A_{μ} and B_z . In Fig. 3 we show the 2-dim latent space for the popular MNIST digits (LeCun & Cortes, 2010) during training (4 leftmost panels). The three archetypes, mapped into the corners of the simplex, are ‘0’, ‘1’ and ‘7’¹.

3. Experiments

3.1. Representation Learning for *Microchiroptera*

Based on expert knowledge *body mass* and *wing aspect ratio* were chosen to be the two most important features relating

¹A detailed implementation is provided in case of acceptance. [http...](http://...)

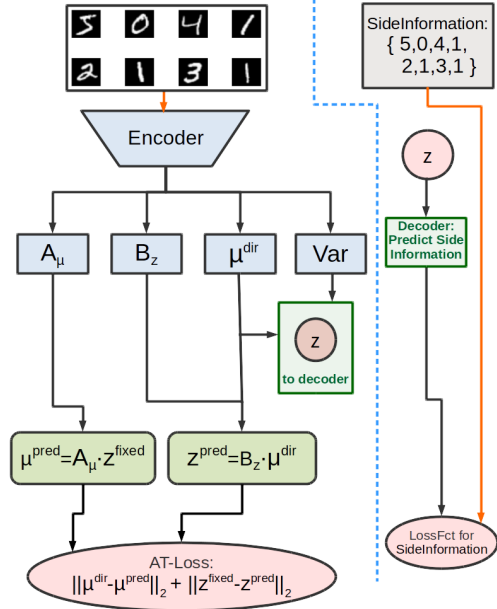


Figure 2. Architecture of *DeepAA* model, Encoder: Weight matrices A_{μ} and B_z are needed in order to estimate the AT-loss in Eq. 11. The branch containing μ^{dir} and Var used to generate random samples z is a simple VAE. In this VAE, enforcing the additional constraints C_1 and C_2 is ensured by adding the branch containing the weight matrices. In case of side information, the branch right of the dotted line depicts the necessary model extension where the latent space need to produce the respective side information as well as the reconstructed input from a single latent variable μ^{dir} . Adding the archetype loss to an existing model requires modifying only the encoder part of a VAE.

to the *dominant food habit* of *Microchiroptera*, see Fig. 1. But (Norberg et al., 1987) have collected six additional measurements on each species. These are *wing span*, *wing area*, *wing loading*, *tip length ratio*, *tip area ratio* and *tip shape index*. Arguably, more meaningful archetypes may be found by learning an appropriate representation based on *all* available measurements. We use *DeepAA* to learn such a representation. Our encoder is shown in Fig. 2. Both encoder and decoder are parametrized by two feed-forward neural networks with two hidden layers each. We train the VAE for 200 epochs (learning rate: 1e-3, batch size: 60) in a side information setting with the *dominant food habit* as the additional information. In order to compare to the results based on linear AA, we choose the same number of archetypes as in Fig. 1. The representation learned by *DeepAA* is shown in Fig. 4. By running the latent *Archetypes A*, *B* and *C* through the decoder of our trained VAE we obtain three sets of eight *generated* features. Each set represents the traits of

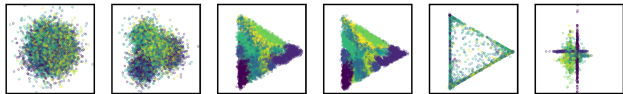


Figure 3. Latent space simplex during training of *DeepAA* on MNIST after 1, 2, 60 and 300 epochs (from left to right.) The two rightmost figures show pathological cases. In the first of the two cases, the influence of the Archetype Loss was too high (with the divergence set too low) so that the inner of the simplex remains mostly unpopulated. In the second (rightmost) case, the Archetype Loss was too high while the divergence was kept at the same level as in the training of *DeepAA* that produced the first four images.

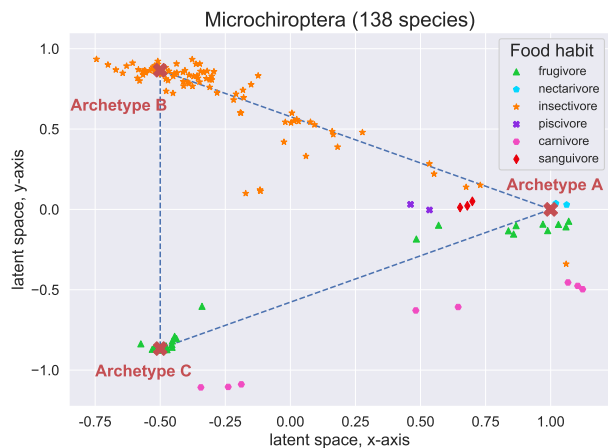


Figure 4. *DeepAA* finds an organisation of species not unsimilar to linear AA: Insectivores and frugivores populate opposite ends of the Pareto front. But the interesting insight is the representation associated with the latent space ordering found by *DeepAA*. While linear AA was forced to find the best possible representation in the space of *Wing Aspect Ratio* and *Body Mass*, *DeepAA* was free to learn a representation which included two additional features, i.e. *Wing Loading* and *TipShapeIndex*. Based on these features *DeepAA* was able to learn a richer representation which is in much agreement with the finding of (Norberg et al., 1987), as discussed in the paragraph *Results and Discussion*.

an archetypal species in terms of the eight measures introduced by (Norberg et al., 1987). For these three species we analyze by how much each feature changes. This allows us to deduce the most important measures characterizing the relation between *food habit* and *morphology*.

Results and Discussion Our results are shown in Table 2. For each measure we consider the largest relative change with respect to the archetypes and take the magnitude of these changes as a proxy for feature importance. Similar to Fig. 1, we find that *total mass* is the most important feature: The heavier a bat the more likely it is to be a frugivore – a result consistent with linear AA. But in contrast to the linear case *DeepAA* does not consider *wing aspect ratio*. Instead *wing area* and *wing span* are deemed important. But as *wing*

Table 2. Characteristic traits of the archetypes identified in Fig. 4 and the task each archetypal species is optimized to perform.

MEASURE	IMPORTANCE	A	B	C
TOTAL MASS	35%	MED	LOW	HIGH
WING AREA	30%	LOW	MED	HIGH
WING LOADING	15%	LOW	MED	HIGH
WING SPAN	10%	LOW	LOW	HIGH
TIP SHAPE INDEX	10%	HIGH	MED	LOW

aspect ratio is simply the square of the *wing span* divided by the *wing area*, one could argue that *DeepAA* captures the influence of *wing aspect ratio* nonetheless. A novel insight produced by *DeepAA* is the importance of two additional features, namely *wing loading* and *tip shape index*. According to (Norberg et al., 1987), as wing loading increases, the bat must fly faster and expend more energy, and the range of accessible flight behavior is reduced. As *Archetype A* has low *wing loading*, thereby enabling various flight behaviors, it makes sense that this archetype can accommodate the largest variation in food habits, i.e. frugivore, nectarivore, insectivore, piscivore, carnivore and sanguivore are all found in proximity to *Archetype A*. Regarding *tip shape index*, (Norberg et al., 1987) find that it is inversely correlated with flight speed. They further state that flight speed increases significantly with *wing loading*. As shown in Table 2, this is exactly the inverse relation learned by *DeepAA* – high *wing loading* and low *tip shape index* for *Archetype A* while the inverse is true for *Archetype C*. The learned representation is thus in very good agreement with the various trade-offs found by (Norberg et al., 1987). But *DeepAA* did not only find a richer and arguably more meaningful representation than linear AA, it also learned the appropriate scaling when combining the different features. By contrast, in linear AA one had to know *beforehand* that *total mass* would need to enter the model logarithmically.

3.2. Exploring CelebA without Side Information

DeepAA can be employed to perform unsupervised exploration. As a proof of concept, archetypal faces in the large-scale CelebFaces Attributes (CelebA) dataset (Liu et al., 2015) are explored. The dataset comprises 202599 images of faces with 10177 unique identities.

In our experiments we adopt the "Deep Feature Consistent Variational Autoencoder" proposed by (Hou et al., 2017). Instead of comparing the generated image and input image pixel-wise, the feature perceptual loss is considered as the reconstruction loss. To this end, both input and generated image are processed by a pre-trained VGG convolutional neural network (Simonyan & Zisserman, 2014). The feature perceptual loss is then defined as the sum of the squared ℓ^2 norm of the feature representations at selected hidden layers. In our implementation, we use the VAE-123 model of the

original paper with the modification as depicted in Fig. 2. We train our model with the Adam optimizer (Kingma & Ba, 2014) at a learning rate of 0.0005 and we set the first moment decay rate to $\beta_1 = 0.5$. Training is performed with a batch size of 64 for 10 epochs and 90% of the dataset are used for training while the remaining 10% are reserved for testing.

In order to identify the appropriate number of archetypes (model selection), the information curve (Shamir et al., 2010; Alemi et al., 2016; Wieczorek et al., 2018) is considered. To arrive at this curve, the Lagrange multiplier λ is decreased by 20% every 500 iterations. For a selected number of archetypes, the reconstruction loss against the KL divergence is recorded, with both quantities being evaluated on the test set.

Results and Discussion: In the first Experiment, model selection is performed by considering the reconstruction loss minima of the information curves for different numbers of archetypes given in Fig. 5. The curve starts converging at around 35 archetypes. Higher archetype numbers yield many archetypes which are more and more alike, while lower numbers lead to less diverse archetypes. We hypothesize that the former effect reflects the interplay between the number of archetypes and the batch size, requiring a sufficient number of examples in the mini-batch to identify adequate archetypes. The inferred archetypal faces given in Fig. 6 show distinct variations in pose, sex, age, hair color, facial expression and complexion.

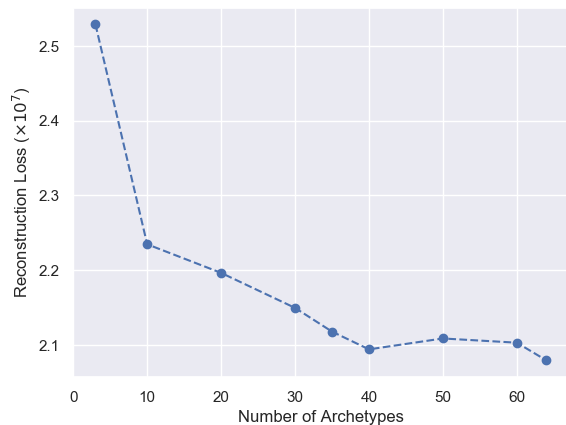


Figure 5. Reconstruction loss with varying number of archetypes. Each point represents the minimum of the information curve with the selected number of archetypes. It is assumed that the maximum number of archetypes should not exceed the batch size of 64.

Intuitively, the pose appears to be a relevant factor of variation in face images. Thus, a pose archetype such as D2 shown in Fig. 6 is plausible since the rotation of a face (while the face remains visible) is only possible to some degree.

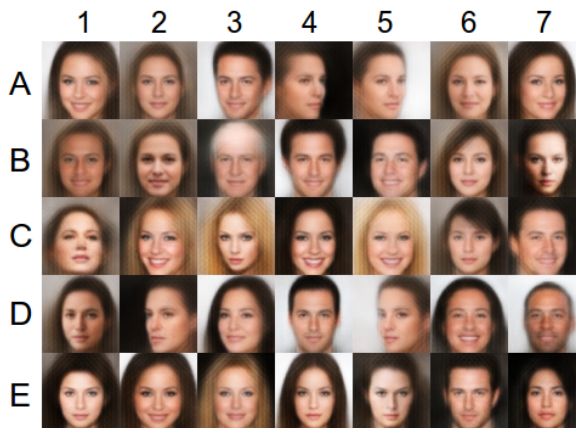


Figure 6. All 35 archetypal faces in CelebA inferred with DeepAA. Distinct variations in pose, sex, age, hair color, facial expression and complexion are captured.

Second Experiment: The latent space is explored by keeping the contribution of an archetype fixed and varying the contributions of other archetypes. In Fig. 7 archetype D2 (pose facing to the left) is held fixed with a weight of $a_{\cdot, D2} = 0.059$ and $a_{\cdot, D2} = 0.508$ while the weights of other archetypes are varied. The results show that the dominant influence of the archetype is observed when the corresponding weight is high. For a lower weight, the influence of the archetype diminishes. Samples with similar compositions of the other archetypes remain similar while only the pose is altered, which illustrates the convex mixture of archetypes. The inferred archetypes can be viewed as single face traits whose convex combination accounts for a great variety of faces in the dataset.

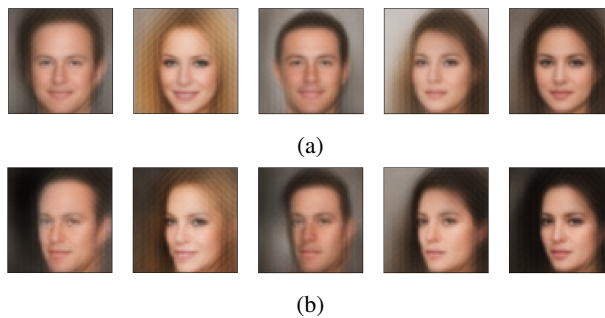


Figure 7. Samples of the latent space for a fixed contribution of archetype D2. The weight of D2 is set to (a) $a_{\cdot, D2} = 0.059$ and (b) $a_{\cdot, D2} = 0.508$. Column-wise, weights are set to $a_{\cdot, j} = 0.15$ for archetypes (i) B3, B4, B5; (ii) C2, C3, C5; (iii) C7, D4, D7; (iv) C6, D3, D5; (v) A1, B2, E7. The remaining weights are chosen uniformly such that all weight assignments sum up to 1. The dominant influence of the pose of D2 is observed in (b) as compared to the smaller contribution in (a). Column-wise, the influence of the remaining archetypes can be observed which lead to similar samples with altered pose.

Third Experiment: An arbitrary sample of the latent space is interpolated towards two archetypes: B3 (bald old male) and C2 (fair-haired female). In Fig. 8 selected interpolation results are shown. By approaching the archetype, characteristic features of the archetypal faces are reinforced. Exploring the archetypes allows to identify directions of variation in the latent space to perform desired convex combinations of different archetypes and enables dataset exploration. Especially in large datasets *DeepAA* can constitute a powerful exploration tool.

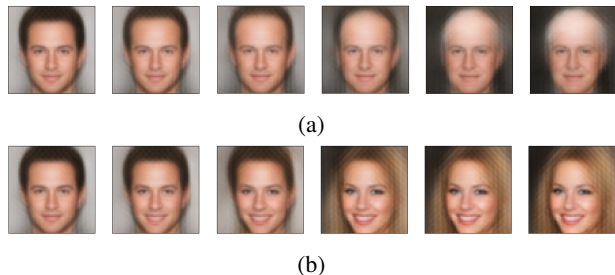


Figure 8. Interpolation sequences from an arbitrary sample of the latent space (first column) towards archetypes (a) B3 and (b) C2. In (a) the evolution of younger male faces to older, bald faces can be observed. In (b) the evolution of dark-haired male faces to fair-haired female faces is displayed.

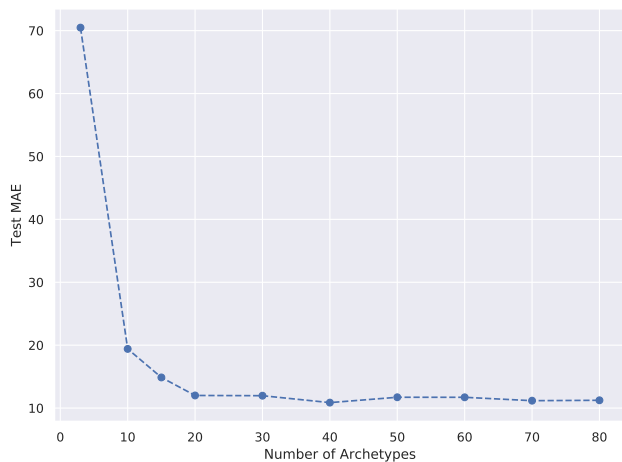


Figure 9. Test MAE with a varying number of archetypes.

3.3. Exploring Chemical Spaces with Side Information

Dataset: As discussed previously, deep archetypal analysis can be considered from a biological point of view. But it is also possible to transfer this principle to other fields such as chemistry. In this experiment, we want to uncover the Pareto front of the chemical space with respect to heat capacity C_v . The chemical space contains all molecules that already exist or can be produced. The heat capacity quantifies the amount

of energy (in Joule) needed to increase 1 Mol of molecules by 1 K at constant volume. Here, a high C_v is especially important for a huge number of applications such as thermal energy storage (Cabeza et al., 2015). In our experiments, we use the QM9 dataset (Ramakrishnan et al., 2014; Ruddigkeit et al., 2012) which was calculated on ab initio DFT method based structures and properties of 134k organic molecules with up to nine atoms (C, O, N, or F), without counting hydrogen.

Set-up: We extracted 204 features for every molecule by using the Chemistry Development Kit (Steinbeck et al., 2003). The neural architectures considered in our experiments have 3 hidden layers with 1024, 512 and 256 neurons, respectively and ReLU activation functions. We train our model in a *supervised* fashion, by reconstructing the molecule and the side information heat capacity, simultaneously. In Experiment 1, we continuously increase the number of latent dimensions to perform model selection. In Experiment 2 and 3, we fix the number of latent dimensions to 19 which corresponds to 20 archetypes. During training, we steadily increase the Lagrange multiplier λ by 1.01 every 500 iterations. Our model is trained with the Adam optimizer (Kingma & Ba, 2014) with an initial learning rate of 0.01. We decay the learning rate with an exponential decay by 0.95 every 10000 iterations. In addition, we use a batch size of 2048 and train the model for 350000 iterations. The dataset is divided in a training and test split of 90/10%.

Results and Discussion: In Experiment 1, we assess the MAE error to estimate the optimal Pareto front when varying the number of archetypes in Fig. 9. In our case, we perform model selection by observing where the MAE converges (starting from 20 archetypes) to select the optimal number of archetypes. Obviously, if the number of archetypes is smaller, it becomes more difficult to reconstruct the data. This stems from the fact there exist a large number of molecules with almost the same heat capacity but with a different shape. Thus, molecules with different shapes are mapped to archetypes with the same heat capacity which makes it hard to resolve the many-to-one mapping in the latent space.

In Experiment 2, we explore the Pareto front to find archetypal molecules that are associated with a particular heat capacity. In this setting, we focus on 20 archetypes (Fig. 9) to obtain the optimal exploration-exploitation trade-off. While focusing only on a small selection of archetypes, we provide the full list in the supplement. In chemistry, the heat capacity is defined as $C_v = \left. \frac{d\epsilon}{dT} \right|_{v=const}$ where ϵ denotes the energy of a molecule and T is the temperature. The energy can be further decomposed into $\epsilon = \epsilon^{Tr} + \epsilon^R + \epsilon^V + \epsilon^E$ where Tr depicts translation, R rotation, V vibration and E the electric contribution, respectively (Atkins & de Paula, 2010; Tinoco, 2002). Building upon this knowledge, we

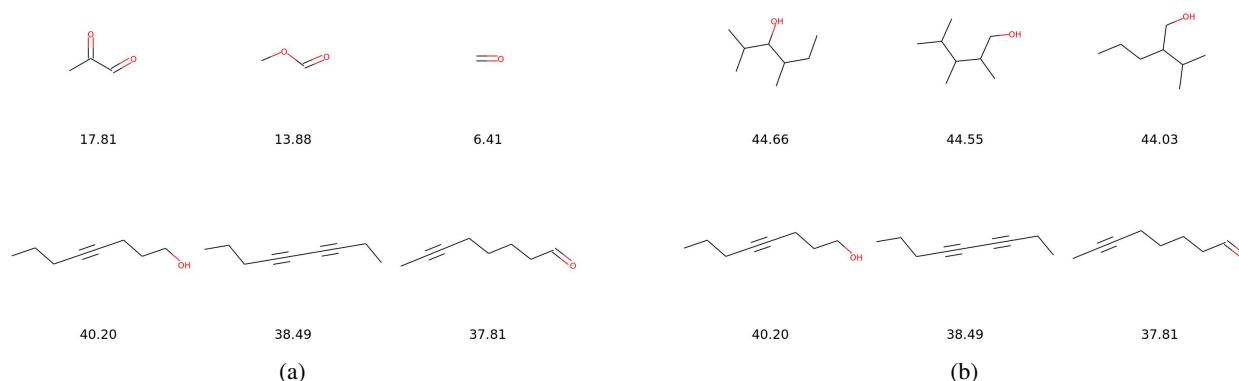


Figure 10. The panels illustrate a comparison between two archetypes where the labels represent the corresponding heat capacity. Here, the columns denote the molecules that are closest to the specific archetype and the rows are the archetypes. Panel a) compares a long chain versus a short chain archetype. Panel b) compares archetypal molecules with the same mass but different shapes.

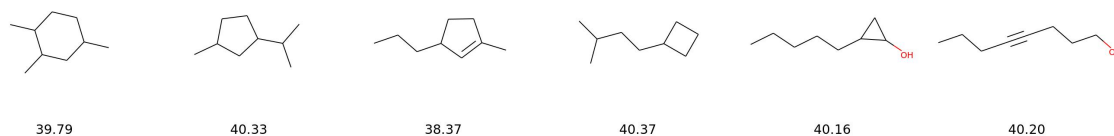


Figure 11. Interpolation between two archetypes produced by our model. The label denote the molecules' heat capacity. While we show only one example, the same results can also be observed for other archetype combinations.

compare different archetypal molecules associated with a particular heat capacity (Fig. 10). Here, the rows correspond to archetypes and the columns depict the three closest test molecules to the archetype. In Fig. 10a we illustrate two archetypes with a high and low heat capacity. The first row archetype has a lower heat capacity because of its shorter chain and more double bonds. Due to these properties, the archetype is more stable which results in a lower vibrational energy V and subsequently in a lower heat capacity. Fig. 10b plots both a non-linear and a linear archetypal molecule with the same atomic mass. Here, the linear molecule loses one of its rotation motions due to its geometry. For this reason, the second row archetype has a lower rotational energy R compared to first row archetype which leads to a lower heat capacity.

Finally, in **Experiment 3**, we focus on the interpolation between two archetypes to justify that molecules cannot lie outside the Pareto front. In doing so, we plot the test samples which are closest to the linear connection between the two archetypes. Here, we observe in Fig. 11 a smooth transition from a ring molecule to a linear molecule with the same heat capacity. That is, a molecule can only change its shape but it cannot go beyond a particular heat capacity which is not part of the Pareto front.

4. Conclusion

In this paper, we introduced a novel approach to explain datapoints as convex combinations of archetypes which is inspired by studies of evolutionary trade-offs. In doing so, we build upon the linear AA approach and combine this concept with the deep IB principle to obtain a non-linear archetype model. In contrast to the classical approach our method offers three advantages: First, our model introduces a data-driven representation learning, which reduces expert knowledge. Second, we learn appropriate transformations when combining features of different types. Third, we are able to incorporate side information into the learning process to identify archetypes with specific properties. Our diverse experiments on biological, vision and chemical datasets demonstrate the applicability of our method in real world settings. For future work, we would like to apply our deep archetype model to text data.

References

- Alemi, A. A., Fischer, I., Dillon, J. V., and Murphy, K. Deep variational information bottleneck. *CoRR*, abs/1612.00410, 2016. URL <http://arxiv.org/abs/1612.00410>.

- Atkins, P. and de Paula, J. *Atkins' Physical Chemistry*. OUP Oxford, 2010. ISBN 9780199543373.
- Bauckhage, C. and Manshaei, K. Kernel archetypal analysis for clustering web search frequency time series. In *2014 22nd International Conference on Pattern Recognition*, pp. 1544–1549, Aug 2014. doi: 10.1109/ICPR.2014.274.
- Bauckhage, C. and Thureau, C. Making archetypal analysis practical. In Denzler, J., Notni, G., and Süße, H. (eds.), *Pattern Recognition*, pp. 272–281. Springer Berlin Heidelberg, 2009. ISBN 978-3-642-03798-6.
- Bauckhage, C., Kersting, K., Hoppe, F., and Thureau, C. Archetypal analysis as an autoencoder. In *Workshop New Challenges in Neural Computation 2015*, pp. 8–16, 10 2015. URL https://www.techfak.uni-bielefeld.de/~fschleif/mlr/mlr_03_2015.pdf.
- Cabeza, L. F., Gutierrez, A., Barreneche, C., Ushak, S., Ángel G. Fernández, Fernández, A. I., and Grageda, M. Lithium in thermal energy storage: A state-of-the-art review. *Renewable and Sustainable Energy Reviews*, 42: 1106 – 1112, 2015. ISSN 1364-0321.
- Canhasi, E. and Kononenko, I. Weighted hierarchical archetypal analysis for multi-document summarization. *Computer Speech & Language*, 37, 11 2015. doi: 10.1016/j.csl.2015.11.004.
- Cutler, A. and Breiman, L. Archetypal analysis. *Technometrics*, 36(4):338–347, 1994. doi: 10.1080/00401706.1994.10485840. URL <http://digitalassets.lib.berkeley.edu/sdtr/ucb/text/379.pdf>.
- Djawdan, M., Sugiyama, T. T., Schlaeger, L. K., Bradley, T. J., and Rose, M. R. Metabolic aspects of the trade-off between fecundity and longevity in *Drosophila melanogaster*. *Physiological Zoology*, 69(5):1176–1195, 1996.
- El Samad, H., Khammash, M., Homescu, C., and Petzold, L. Optimal performance of the heat-shock gene regulatory network. *Proceedings 16th IFAC World Congress*, 16, 1 2005. URL https://engineering.ucsb.edu/~cse/Files/IFACC_HS_OPT04.pdf.
- Garland, T. J. J. Quick guides: Trade-offs. *Current Biology*, 24(2):R60–R61, 2014.
- H. P. Chan, B., Mitchell, D., and Cram, L. Archetypal analysis of galaxy spectra. *Monthly Notices of the Royal Astronomical Society*, 338, 01 2003. doi: 10.1046/j.1365-8711.2003.06099.x.
- Hou, X., Shen, L., Sun, K., and Qiu, G. Deep feature consistent variational autoencoder. In *Applications of Computer Vision (WACV), 2017 IEEE Winter Conference on*, pp. 1133–1141. IEEE, 2017.
- Huggins, P., Pachter, L., and Sturmfels, B. Toward the human genotype. *Bulletin of Mathematical Biology*, 69(8):2723–2735, Nov 2007. doi: 10.1007/s11538-007-9244-7. URL <https://doi.org/10.1007/s11538-007-9244-7>.
- Jang, E., Gu, S., and Poole, B. Categorical Reparameterization with Gumbel-Softmax. *International Conference on Learning Representations (ICLR)*, 2017.
- Kaufmann, D., Keller, S., and Roth, V. Copula archetypal analysis. In Gall, J., Gehler, P., and Leibe, B. (eds.), *Pattern Recognition*, pp. 117–128. Springer International Publishing, 2015. ISBN 978-3-319-24947-6.
- Kingma, D. P. and Ba, J. Adam: A method for stochastic optimization. abs/1412.6980, 2014.
- Kingma, D. P. and Welling, M. Auto-encoding variational bayes. *CoRR*, abs/1312.6114, 2013.
- Kingma, D. P., Mohamed, S., Rezende, D. J., and Welling, M. Semi-supervised learning with deep generative models. In *Advances in Neural Information Processing Systems 27: Annual Conference on Neural Information Processing Systems 2014, December 8-13 2014, Montreal, Quebec, Canada*, pp. 3581–3589, 2014.
- LeCun, Y. and Cortes, C. MNIST handwritten digit database. 2010. URL <http://yann.lecun.com/exdb/mnist/>.
- Liu, Z., Luo, P., Wang, X., and Tang, X. Deep learning face attributes in the wild. In *Proceedings of International Conference on Computer Vision (ICCV)*, December 2015.
- Norberg, U. M., Rayner, J. M. V., and Lighthill, M. J. Ecological morphology and flight in bats (mammalia; chiroptera): wing adaptations, flight performance, foraging strategy and echolocation. *Philosophical Transactions of the Royal Society of London. B, Biological Sciences*, 316(1179), 1987. URL <https://royalsocietypublishing.org/doi/abs/10.1098/rstb.1987.0030>.
- Parbhoo, S., Wieser, M., and Roth, V. Cause-Effect Deep Information Bottleneck For Incomplete Covariates. *arXiv e-prints*, art. arXiv:1807.02326, July 2018.
- Prabhakaran, S., Raman, S., Vogt, J. E., and Roth, V. Automatic model selection in archetype analysis. In Pinz, A., Pock, T., Bischof, H., and Leberl, F. (eds.), *Pattern Recognition*, pp. 458–467. Springer Berlin Heidelberg, 2012. ISBN 978-3-642-32717-9.
- Ramakrishnan, R., Dral, P. O., Rupp, M., and von Lilienfeld, O. A. Quantum chemistry structures and properties of 134 kilo molecules. *Scientific Data*, 1, 2014.

- Rezende, D. and Mohamed, S. Variational inference with normalizing flows. In Bach, F. and Blei, D. (eds.), *Proceedings of the 32nd International Conference on Machine Learning*, volume 37 of *Proceedings of Machine Learning Research*, pp. 1530–1538, Lille, France, 07–09 Jul 2015. PMLR.
- Rezende, D. J., Mohamed, S., and Wierstra, D. Stochastic backpropagation and approximate inference in deep generative models. 32(2):1278–1286, 22–24 Jun 2014.
- Ruddigkeit, L., van Deursen, R., Blum, L. C., and Reymond, J.-L. Enumeration of 166 billion organic small molecules in the chemical universe database gdb-17. *Journal of Chemical Information and Modeling*, 52(11):2864–2875, 2012. doi: 10.1021/ci300415d. URL <https://pubs.acs.org/doi/10.1021/ci300415d>. PMID: 23088335.
- Schuetz, R., Zamboni, N., Zampieri, M., Heinemann, M., and Sauer, U. Multidimensional optimality of microbial metabolism. *Science (New York, N.Y.)*, 336:601–4, 05 2012. doi: 10.1126/science.1216882.
- Seth, S. and Eugster, M. J. A. Probabilistic archetypal analysis. *Machine Learning*, 102(1):85–113, Jan 2016. doi: 10.1007/s10994-015-5498-8. URL <https://doi.org/10.1007/s10994-015-5498-8>.
- Shamir, O., Sabato, S., and Tishby, N. Learning and generalization with the information bottleneck. *Theoretical Computer Science*, 411(29-30):2696–2711, 2010.
- Shoval, O., Sheftel, H., Shinar, G., Hart, Y., Ramote, O., Mayo, A., Dekel, E., Kavanagh, K., and Alon, U. Evolutionary trade-offs, pareto optimality, and the geometry of phenotype space. *Science*, 336(6085):1157–1160, 2012. doi: 10.1126/science.1217405. URL <http://science.sciencemag.org/content/336/6085/1157>.
- Simonyan, K. and Zisserman, A. Very deep convolutional networks for large-scale image recognition. *arXiv preprint arXiv:1409.1556*, 2014.
- Steinbeck, C., Han, Y. Q., Kuhn, S., Horlacher, O., Luttmann, E., and Willighagen, E. The Chemistry Development Kit (CDK): An open-source Java library for chemo- and bioinformatics. *Journal of Chemical Information and Computer Sciences*, 43(2):493–500, 2003.
- Steuer, R. *Multiple Criteria Optimization: Theory, Computation and Application*. John Wiley & Sons, 1986.
- Tendler, A., Mayo, A., and Alon, U. Evolutionary trade-offs, pareto optimality and the morphology of ammonite shells. *BMC Systems Biology*, 9(1), 2015. doi: 10.1186/s12918-015-0149-z. URL <https://doi.org/10.1186/s12918-015-0149-z>.
- Tinoco, I. *Physical Chemistry: Principles and Applications in Biological Sciences*. Number S. 229-313 in *Physical Chemistry: Principles and Applications in Biological Sciences*. Prentice Hall, 2002. ISBN 9780130959430.
- Tishby, N., Pereira, F. C., and Bialek, W. The information bottleneck method. *arXiv preprint physics/0004057*, 2000a.
- Tishby, N., Pereira, F. C., and Bialek, W. The information bottleneck method. *arXiv preprint physics/0004057*, 2000b.
- Wieczorek, A., Wieser, M., Murezzan, D., and Roth, V. Learning Sparse Latent Representations with the Deep Copula Information Bottleneck. *arXiv e-prints*, art. arXiv:1804.06216, April 2018.